Geochemical portray of the Pacific Ridge: New isotopic data and statistical techniques

Cédric Hamelin [a,*], Laure Dosso [b], Barry B. Hanan [c], Manuel Moreira [d], Andrew P. Kositsky [e], Marion Y. Thomas [e]

[a] I.U.E.M., U.B.O., Place Nicolas Copernic, 29280 Plouzané, France
[b] Centre National de la Recherche Scientifique, UMR 6538, IFREMER, BP70, 29280 Plouzané, France
[c] Department of Geological Sciences, S.D.S.U., 5500 Campanile Drive, San Diego, CA 92182-1020, USA
[d] Institut de Physique du Globe de Paris, CNRS UMR 7154, 1 rue Jussieu, 75252 Paris CEDEX 05, France
[e] Tectonics Observatory, California Institute of Technology, Pasadena, CA 91125, USA

ARTICLE INFO

ABSTRACT

Samples collected during the PACANTARCTIC 2 cruise fill a sampling gap from 53° to 41° S along the Pacific Antarctic Ridge (PAR). Analysis of Sr, Nd, Pb, Hf, and He isotope compositions of these new samples is shown together with published data from 66°S to 53°S and from the EPR. The recent advance in analytical mass spectrometry techniques generates a spectacular increase in the number of multidimensional isotopic data for oceanic basalts. Working with such multidimensional datasets generates a new approach for the data interpretation, preferably based on statistical analysis techniques.

Principal Component Analysis (PCA) is a powerful mathematical tool to study this type of datasets. The purpose of PCA is to reduce the number of dimensions by keeping only those characteristics that contribute most to its variance. Using this technique, it becomes possible to have a statistical picture of the geochemical variations along the entire Pacific Ridge from 70°S to 10°S. The incomplete sampling of the ridge led previously to the identification of a large-scale division of the south Pacific mantle at the latitude of Easter Island. The PCA method applied here to the completed dataset reveals a different geochemical profile. Along the Pacific Ridge, a large-scale bell-shaped variation with an extremum at about 38°S of latitude is interpreted as a progressive change in the geochemical characteristics of the depleted matrix of the mantle. This Pacific Isotopic Bump (PIB) is also noticeable in the He isotopic ratio along-axis variation. The linear correlation observed between He and heavy radiogenic isotopes, together with the result of the PCA calculation, suggests that the large-scale variation is unrelated to the plume–ridge interactions in the area and should rather be attributed to the partial melting of a marble-cake assemblage.

© 2010 Elsevier B.V. All rights reserved.

1. Introduction

Mid-oceanic ridge basalts (MORB) are the result of continuous melting of the ambient upper mantle beneath oceanic ridges. The MORB-source mantle is generally thought to have been depleted ~2 Gy ago by extraction of the continents. Although the range of geochemical variations in oceanic basalts is mostly attributed to the influence of Ocean Island Basalt (OIB), significant geochemical heterogeneity in MORB has been recognized (Hofmann, 2003 and reference therein; Rudge et al., 2005). This heterogeneity has been revealed using radiogenic isotope ratios (Sr, Nd, Pb, and Hf) in areas devoid of plume influence. Numerous studies have attempted to model the mixing relationship between enriched and depleted domains within the mantle to reproduce the range of isotopic variations observed in oceanic basalts (Albarède, 2001; Kellogg et al., 2007; Meibom and Anderson, 2004;

Rudge et al., 2005). The range of Sr, Nd, and Pb isotopic compositions depends not only on the end-member compositions but also on the volume of mantle sampled during the melting relative to the length scale of heterogeneities (Kellogg et al., 2007). Therefore, the range of MORB geochemical variations reflects the size, the spatial distribution, and the difference of fusibility of heterogeneities within the upper mantle. In addition to this intrinsic heterogeneity of the MORB mantle, radiogenic isotope studies have led to the definition of distinct broad mantle isotopic domains, such as the archetypal DUPAL anomaly located in the south hemisphere (Castillo, 1998; Dupré and Allègre, 1983). Boundaries between these domains can be (i) extremely sharp as seen at the Antarctic Australian–Antarctic Discordance (ADD), with isotopic ratios (Sr, Nd, Pb, and Hf) abruptly changing from Indian to Pacific values (Cooper et al., 2009, Hanan et al., 2004; Meyzen et al., 2007; Pyle et al., 1992) or (ii) more gradual as seen in the transition from Southwest Indian Ridge to South Atlantic MORB (Meyzen et al, 2005).

Another example of these large geochemical provinces is given by the two sub-pacific mantle domains (Vlastélic et al., 1999). The distinctive isotopic properties of these large-scale geochemical domains suggest a

* Corresponding author. I.P.G.P, 1 rue Jussieu, Bureau 345, 75252 Paris CEDEX 05, France. Tel.: +33 1 83 95 76 72; fax: +33 1 7193 7710.
E-mail address: hamelin@ipgp.fr (C. Hamelin).

long-term isolation of these mantle provinces, each with its own convective histories involving various amounts of melting residues and recycled components. On the basis of an incomplete dataset, a boundary between these two pacific provinces has been located at the latitude of the Easter Island microplate (Vlastélic et al., 1999). But in order to have a complete geochemical view of the southern Pacific Ridge from 66 to 10°S, it was necessary to fill the sampling gap between 53°S and 41°S. This became one of the main objectives of the PACANTARCTIC2 cruise, which took place in 2004–05 (Dosso et al. 2005, Hamelin et al., 2010, Klingelhoefer et al., 2006; Moreira et al., 2008). Analyses of Sr, Nd, Pb, Hf, and He isotopic compositions of these new samples from the Pacific Antarctic Ridge (PAR) are compiled here together with published data from 66°S to 53°S and from the East Pacific Rise (EPR). Therefore, it becomes possible to have a picture of the geochemical variations along the entire Pacific Ridge from 66°S to the 10°S. Adapting a Principal Component Analysis (PCA) to incomplete datasets, we show a detailed portray of the geochemical variability of the Pacific Ridge.

2. Data selection and analytical methods

2.1. The Pacific Ridge database from 10 to 66°S

Along the Pacific Ridge, the Chile Triple Junction at 35°S/110°W separates the PAR from the EPR. The two pacific ridges show different geological settings: the full spreading rate increases along the PAR from 54 mm/yr at 65°S to 100 mm/yr at 35°S, whereas it decreases along the EPR from 158 mm/yr at 35°S to 146 mm/yr at 10°S. In conjunction, the ridge axis morphology changes from a valley to a dome north of 60°S along the PAR (Ondréas et al., 2001), whereas the EPR is characterized by a uniform dome shaped morphology. Three plume–ridge interactions generate abnormal morphological structures along this section: Foundation (~38°S), Easter Island (~26°S) and 17°S. They are recognized by a high ridge cross-sectional area (Klingelhöfer et al., 2006) and the presence of intense off-axis volcanic activity. Compared to the EPR, the Pacific Antarctic Ridge still remains geochemically poorly known. A large portion of this plate boundary has been previously surveyed (Cande et al., 1995; Lonsdale, 1994), but the northern part has only recently been sampled (Dosso et al., 2005; Hamelin et al., 2010; Moreira et al., 2008).

To generate a coherent database along the pacific ridges, on-axis samples analyzed for one or more isotopic ratios (Sr–Nd–Pb–Hf–He) are selected from 66°S to 10°S using our new isotope data (Table 1) completed with the petrological database of the Lamont-Doherty Earth Observatory (http://www.petdb.org). In most cases when the reference values of the standards are reported, the data are normalized to the values of NBS987, 0.71025 for Sr, of JNdi-1, 0.512104 and La Jolla, 0.511852 for Nd, NBS981, $^{206}Pb/^{204}Pb = 16.9373$, $^{207}Pb/^{204}Pb = 15.4925$, $^{208}Pb/^{204}Pb = 36.7054$, for Pb and JMC475, 0.282162 for Hf (see http://georem.mpch-mainz.gwdg.de/ for details and references).

2.2. Analytical methods

2.2.1. Double Spike Pb analyses along the PAR

New high-resolution Pb analyses were carried out for samples collected during PACANTARCTIC1 (PAC1) and PACANTARCTIC2 (PAC2) cruises along PAR segments from 66°S to 56°S and from 53°S to 41°S, respectively (Fig. 1 and Table 1). Small chips from the inner part of the pillow lavas were handpicked to avoid altered surfaces that could be a potential source of Pb contamination. Powdered samples were leached with 6 M HCl at 140 °C for an hour and then rinsed up to 6 times with ultrapure water prior to dissolution. Lead separation was then performed on an anionic exchange resin. Pb analyses were performed at Ifremer (Centre de Brest) on a Finnigan MAT 26x multicollector instrument (MAT261 upgraded by Spectromat), using the double spike technique with the calibrated Southampton-Brest 207/204 spike (Ishizuka et al., 2003).

Replicate analyses of the Pb isotope standard NBS981 gave an average of 16.9432 ± 0.0027 and 15.5004 ± 0.0029 and 36.7326 ± 0.0086 for $^{206}Pb/^{204}Pb$, $^{207}Pb/^{204}Pb$, and $^{208}Pb/^{204}Pb$, respectively. Pb blanks measured using this procedure were <100 pg and thus negligible relative to the amount of sample analyzed.

2.2.2. Hf measurements along the PAR

Hafnium isotopic compositions were analyzed along the PAC1 ridge segments at SDSU on splits from the same samples (Hamelin et al., 2010). Hf was separated using the protocol of Blichert-Toft et al., 1997 with a negligible blank of less than 25 pg. Hf isotope ratios were measured at SDSU using the Nu Plasma. The $^{176}Hf/^{177}Hf$ was normalized for mass fractionation relative to $^{179}Hf/^{177}Hf = 0.7325$. The JMC-475 Hf standard $^{176}Hf/^{177}Hf$ gave 0.282160 ± 0.000010 (2σ) during this study. The standard was run alternately with samples to monitor machine performance.

2.2.3. He measurements along the PAR

Helium isotopic compositions have been measured on PAC1 and PAC2 samples at IPGP (Institut de Physique du Globe de Paris). Fresh pieces of glass were cleaned with distilled water, ethanol, and acetone using an ultrasonic bath. Some samples were also cleaned with hydrogen peroxide in order to remove some Mg crust. Analytical procedure is identical to previous studies from our laboratory and can be found in Moreira et al. (1995). Samples were crushed under vacuum with analytical blanks of 7 ± 1 nccSTP ^4He. This corresponds to 0.02 to 0.4% of the samples. Helium concentrations and isotopic composition were measured using the ARESIBOII mass spectrometer (Moreira et al., 2008).

3. New results compared to published MORB data along this ridge section

These results include samples from 66°S to 56°S (PAC1) and from 53°S to 41°S (PAC2) (Fig. 1). New high-resolution Pb analyses as well as Hf and He analyses are presented here in Table 1. The Sr, Nd, and Hf analyses on the same samples are found in Vlastélic et al. (2000) and Hamelin et al. (2010).

3.1. Binary isotopic correlations

With 7 isotopic ratios, the number of possible binary isotope diagrams is 21. As an example, we choose here to describe 4 such binary plots, selecting some of the most commonly discussed (Fig. 2A–D). In all diagrams, pacific MORB samples devoid of plume influence define linear correlations that in most cases have been previously described in the literature. This result is in good agreement with the expected coherence in behavior between Rb–Sr, U–Pb, Th–Pb, Sm–Nd, and Lu–Hf isotopic systems compared to each other during magmatic processes. When plume–ridge interaction samples are included in our dataset, they define elongated fields overlapping PAR-EPR array except in Fig. 2C where He-ε_{Nd} isotopic ratios define sub-parallel trends, which emerge from the PAR-EPR array and point towards higher $^3He/^4He$ (R/Ra) ratios. More than 30 years of He isotopes systematic of oceanic basalts worldwide have shown that MORB samples are characterized by a narrow range of composition compared to OIB samples. However even within this limited range, our data show a linear correlation between $^3He/^4He$ (R/Ra) values and ε_{Nd} (Fig. 2C). The correlation between He and other isotopic systems will be discussed further below (Section 4.4.2).

In contrast with the decoupling of Hf and Nd isotope compositions previously documented in MORB (e.g., Chauvel and Blichert-Toft, 2001; Debaille et al., 2006; Patchett and Tatsumoto, 1980; Salters and White, 1998), a rather good correlation between these two isotopic systems is observed along our studied are (Fig. 2B). Debaille et al. (2006) have suggested that a distinctive behavior of Hf during disequilibrium melting along their studied ride area (Atlantic ridge

Table 1
Complete Sr, Nd, Pb, Hf, and He isotope data table for PACANTARCTIC 1 and 2 samples. In italic font, previously published data (Hamelin et al., 2010; Moreira et al., 2008; Vlastélic et al., 1999, 2000).

|	$^{87}Sr/^{86}Sr$	$^{143}Nd/^{144}Nd$	εNd	$^{206}Pb/^{204}Pb$	$^{207}Pb/^{204}Pb$	$^{208}Pb/^{204}Pb$	$^{176}Hf/^{177}Hf$	εHf	$^{3}He/^{4}He$	Long. (°)	Lat. (°)	Depth
PACANTARCTIC 2												
PAC2DR38-1	*0.702465*	*0.513108*	*9.17*	*18.671*	*15.533*	*38.039*	*0.283125*	*12.50*	*7.2*	−111.3	−41.80	2524
PAC2DR37-1	*0.702462*	*0.513091*	*8.84*	*18.722*	*15.540*	*38.110*	*0.283106*	*11.80*	*7.3*	−111.3	−42.27	2475
PAC2DR37-2							*0.283118*	*12.25*	*7.3*	−111.3	−42.27	2475
PAC2DR36-1	*0.702479*	*0.513066*	*8.34*	*18.724*	*15.538*	*38.117*	*0.283119*	*12.27*	*7.5*	−111.6	−42.95	2503
PAC2DR35-1a							*0.283121*	*12.34*	*7.2*	−111.8	−43.59	2463
PAC2DR35-2	*0.702492*	*0.513097*	*8.95*	*18.736*	*15.550*	*38.146*	*0.283127*	*12.54*	*7.2*	−111.8	−43.59	2463
PAC2DR34-1	*0.702392*	*0.513108*	*9.17*	*18.798*	*15.549*	*38.234*	*0.283145*	*13.20*	*7.3*	−112.0	−44.24	2467
PAC2DR33-1	*0.702488*	*0.513082*	*8.66*	*18.817*	*15.562*	*38.236*	*0.283111*	*11.99*	*7.26*	−112.3	−44.87	2374
PAC2DR32-1	*0.702516*	*0.513078*	*8.58*	*18.809*	*15.539*	*38.202*	*0.283100*	*11.60*	*7.2*	−112.4	−45.39	2384
PAC2DR31-3	*0.702479*	*0.513066*	*8.36*	*18.833*	*15.554*	*38.242*	*0.283112*	*12.03*	*7.3*	−112.7	−45.85	2414
PAC2DR30-1	*0.702472*	*0.513060*	*8.24*	*18.887*	*15.565*	*38.311*	*0.283106*	*11.83*	*6.8*	−112.9	−46.40	2345
PAC2DR29-1	*0.702504*	*0.513059*	*8.22*	*18.798*	*15.538*	*38.208*	*0.283117*	*12.19*	*7.2*	−113.1	−47.01	2407
PAC2DR28-2	*0.702468*	*0.513070*	*8.43*	*18.725*	*15.539*	*38.121*	*0.283102*	*11.66*	*7.1*	−113.3	−47.51	2489
PAC2DR27-2	*0.702643*	*0.513035*	*7.74*	*19.168*	*15.581*	*38.624*	*0.283094*	*11.37*	*6.1*	−113.4	−48.18	2359
PAC2DR22-1	*0.702465*	*0.513100*	*9.01*	*18.726*	*15.539*	*38.153*	*0.283131*	*12.69*	*7.25*	−113.6	−48.73	2413
PAC2DR22-3	*0.702468*			*18.761*	*15.540*	*38.202*	*0.283130*	*12.68*		−113.6	−48.73	2413
PAC2DR21-2	*0.702483*	*0.513088*	*8.78*	*18.768*	*15.544*	*38.189*	*0.283125*	*12.48*	*7.1*	−113.8	−49.26	2339
PAC2DR9-1	*0.702499*	*0.513088*	*8.78*	*18.768*	*15.540*	*38.202*	*0.283122*	*12.37*		−117.0	−49.59	2380
PAC2DR9-2				*18.798*	*15.552*	*38.244*	*0.283132*	*12.73*		−117.0	−49.59	2380
PAC2DR20-1	*0.702493*	*0.513092*	*8.86*	*18.749*	*15.540*	*38.168*	*0.283126*	*12.51*	*7.1*	−116.8	−49.73	2441
PAC2DR8-1	*0.702483*	*0.513077*	*8.56*	*18.796*	*15.550*	*38.237*	*0.283132*	*12.74*	*7.3*	−117.1	−49.99	2221
PAC2DR8-2				*18.670*	*15.535*	*38.031*	*0.283140*	*13.03*		−117.1	−49.99	2221
PAC2DR7-4	*0.702449*	*0.513088*	*8.78*	*18.741*	*15.528*	*38.148*	*0.283135*	*12.84*	*7.4*	−117.2	−50.25	2229
PAC2DR6-1	*0.702518*	*0.513094*	*8.90*	*18.792*	*15.543*	*38.201*	*0.283133*	*12.75*		−117.2	−50.70	2610
PAC2DR6-6	*0.702396*	*0.513099*	*8.99*	*18.696*	*15.537*	*38.123*	*0.283143*	*13.12*		−117.2	−50.70	2610
PAC2DR5-2g	*0.702524*	*0.513098*	*8.97*	*18.674*	*15.537*	*38.110*	*0.283135*	*12.85*	*7.5*	−117.4	−50.98	2784
PAC2DR4-2	*0.702367*	*0.513134*	*9.68*	*18.531*	*15.513*	*37.942*	*0.283163*	*13.83*	*7.7*	−117.8	−51.43	2409
PAC2DR3-1										−118.0	−51.79	2397
PAC2DR3-3	*0.702382*	*0.513112*	*9.25*	*18.701*	*15.526*	*38.092*	*0.283143*	*13.12*	*7.5*	−118.0	−51.79	2397
PAC2DR2	*0.702417*	*0.513116*	*9.32*	*18.724*	*15.530*	*38.110*	*0.283141*	*13.06*		−118.1	−52.13	2405
PAC2DR1-1	*0.702422*	*0.513090*	*8.81*	*18.822*	*15.547*	*38.199*	*0.283133*	*12.75*	*7.6*	−118.4	−52.53	2323
PACANTARCTIC 1												
PAC1DR14-2	*0.702538*	*0.513138*	*9.75*	*18.494*	*15.489*	*38.100*	*0.283225*	*16.02*	*7.6*	−145.09	−56.00	2617
PAC1DR14-3	*0.702530*	*0.513102*	*9.05*	*18.776*	*15.524*	*38.379*	*0.283214*	*15.63*		−145.09	−56.00	2617
PAC1DR14-4	*0.702557*	*0.513131*	*9.62*	*18.769*	*15.523*	*38.370*	*0.283218*	*15.77*		−145.09	−56.00	2617
PAC1DR13-2g	*0.702556*	*0.513142*	*9.82*	*18.508*	*15.503*	*37.954*	*0.283204*	*15.28*	*7.6*	−145.74	−56.57	2674
PAC1DR13-3	*0.702570*	*0.513145*	*9.89*	*18.508*	*15.505*	*37.963*	*0.283200*	*15.14*		−145.74	−56.57	2674
PAC1DR12-1g	*0.702310*	*0.513150*	*9.99*	*18.064*	*15.467*	*37.468*	*0.283235*	*16.37*		−146.29	−57.18	2539
PAC1DR12-3g	*0.702375*	*0.513146*	*9.91*	*18.194*	*15.473*	*37.627*	*0.283217*	*15.74*		−146.29	−57.18	2539
PAC1DR12-3r	*0.702395*	*0.513170*	*10.38*	*18.192*	*15.470*	*37.620*	*0.283216*	*15.70*		−146.29	−57.18	2539
PAC1DR11-1g	*0.702435*	*0.513125*	*9.50*	*18.420*	*15.491*	*37.877*	*0.283171*	*14.11*		−146.80	−57.63	2500
PAC1DR11-3	*0.702469*	*0.513129*	*9.58*	*18.397*	*15.491*	*37.816*	*0.283182*	*14.50*		−146.80	−57.63	2500
PAC1DR10-1g	*0.702473*	*0.513112*	*9.25*	*18.426*	*15.492*	*37.881*	*0.283149*	*13.33*		−148.50	−57.89	2319
PAC1DR10-3	*0.702470*	*0.513127*	*9.54*	*18.400*	*15.483*	*37.798*	*0.283148*	*13.30*		−148.50	−57.89	2319
PAC1DR09-g	*0.702467*	*0.513120*	*9.40*	*18.638*	*15.511*	*38.075*	*0.283150*	*13.37*		−149.14	−58.85	2484
PAC1DR09-1	*0.702372*	*0.513112*	*9.25*	*18.376*	*15.470*	*37.819*				−149.14	−58.85	2484
PAC1DR08-2	*0.702388*	*0.513110*	*9.21*	*18.406*	*15.480*	*37.827*	*0.283150*	*13.37*		−150.02	−59.5	2365
PAC1DR08-3	*0.702376*	*0.513113*	*9.27*	*18.398*	*15.475*	*37.809*	*0.283149*	*13.33*	*7.8*	−150.02	−59.5	2365
PAC1DR07-1g	*0.702472*	*0.513099*	*8.99*	*18.609*	*15.505*	*38.039*	*0.283144*	*13.16*		−152.08	−60.00	2362
PAC1DR07-2g	*0.702454*	*0.513098*	*8.97*	*18.620*	*15.509*	*38.062*	*0.283129*	*12.63*		−152.08	−60.00	2362
PAC1DR07-3	*0.702428*	*0.513090*	*8.82*	*18.631*	*15.501*	*38.041*	*0.283132*	*12.73*		−152.08	−60.00	2362
PAC1DR06-g	*0.702502*	*0.513126*	*9.52*	*18.498*	*15.491*	*37.911*	*0.283163*	*13.83*	*8*	−153.21	−60.94	2527
PAC1DR06-2	*0.702389*	*0.513113*	*9.27*	*18.491*	*15.493*	*37.912*	*0.283171*	*14.11*		−153.21	−60.94	2527
PAC1DR05-1g	*0.702407*	*0.513132*	*9.64*	*18.489*	*15.495*	*37.926*	*0.283168*	*14,00*		−154.54	−62.00	2344
PAC1DR05-3	*0.702435*	*0.513138*	*9.75*	*18.490*	*15.496*	*37.936*	*0.283179*	*14.39*	*7.9*	−154.54	−62.00	2344
PAC1DR05-r	*0.702455*	*0.513122*	*9.44*	*18.482*	*15.488*	*37.904*	*0.283183*	*14.53*		−154.54	−62.00	2344
PAC1DR03-1	*0.702421*	*0.513107*	*9.15*	*18.505*	*15.498*	*37.974*	*0.283152*	*13.44*	*7.3*	−156.08	−62.32	2219
PAC1DR03-2	*0.702439*	*0.513106*	*9.13*	*18.498*	*15.494*	*37.965*	*0.283147*	*13.26*	*7.3*	−156.08	−62.32	2219
PAC1DR02-g	*0.702335*	*0.513141*	*9.81*	*18.272*	*15.511*	*37.837*	*0.283189*	*14.75*		−156.54	−62.64	2489
PAC1DR02-1	*0.702362*	*0.513147*	*9.93*	*18.369*	*15.498*	*37.860*	*0.283186*	*14.64*		−156.54	−62.64	2489
PAC1CV09	*0.702370*	*0.513110*	*9.21*	*18.236*	*15.588*	*38.063*	*0.283139*	*12.98*		−159.61	−62.66	2714
PAC1CV08	*0.702419*	*0.513112*	*9.25*	*18.487*	*15.503*	*37.965*	*0.283126*	*12.52*		−162.44	−62.77	2534
PAC1CV06-r	*0.702362*	*0.513128*	*9.56*	*18.344*	*15.475*	*37.787*	*0.283169*	*14.04*		−166.06	−63.45	2755
PAC1CV06-g	*0.702397*	*0.513129*	*9.58*	*18.350*	*15.476*	*37.804*	*0.283172*	*14.15*		−166.06	−63.45	2755
PAC1CV04-g	*0.702512*	*0.513144*	*9.87*	*18.157*	*15.462*	*37.575*	*0.283173*	*14.18*	*8.1*	−169.40	−64.4	2340
PAC1CV03-r	*0.702423*	*0.513109*	*9.19*	*18.475*	*15.501*	*37.952*	*0.283173*	*14.18*		−171.88	−64.53	2576
PAC1CV03-g	*0.702406*	*0.513117*	*9.34*	*18.492*	*15.486*	*37.923*	*0.283170*	*14.07*		−171.88	−64.53	2576
PAC1CV02-g	*0.702568*	*0.513135*	*9.69*	*18.391*	*15.485*	*37.868*	*0.283175*	*14.25*	*7.6*	−172.43	−64.83	2936
PAC1CV01-r	*0.702551*	*0.513153*	*10.05*	*18.447*	*15.557*	*38.121*	*0.283156*	*13.58*		−173.75	−65.10	2863
PAC1CV01-g	*0.702597*	*0.513124*	*9.48*	*18.761*	*15.591*	*38.549*	*0.283144*	*13.16*		−173.75	−65.10	2863
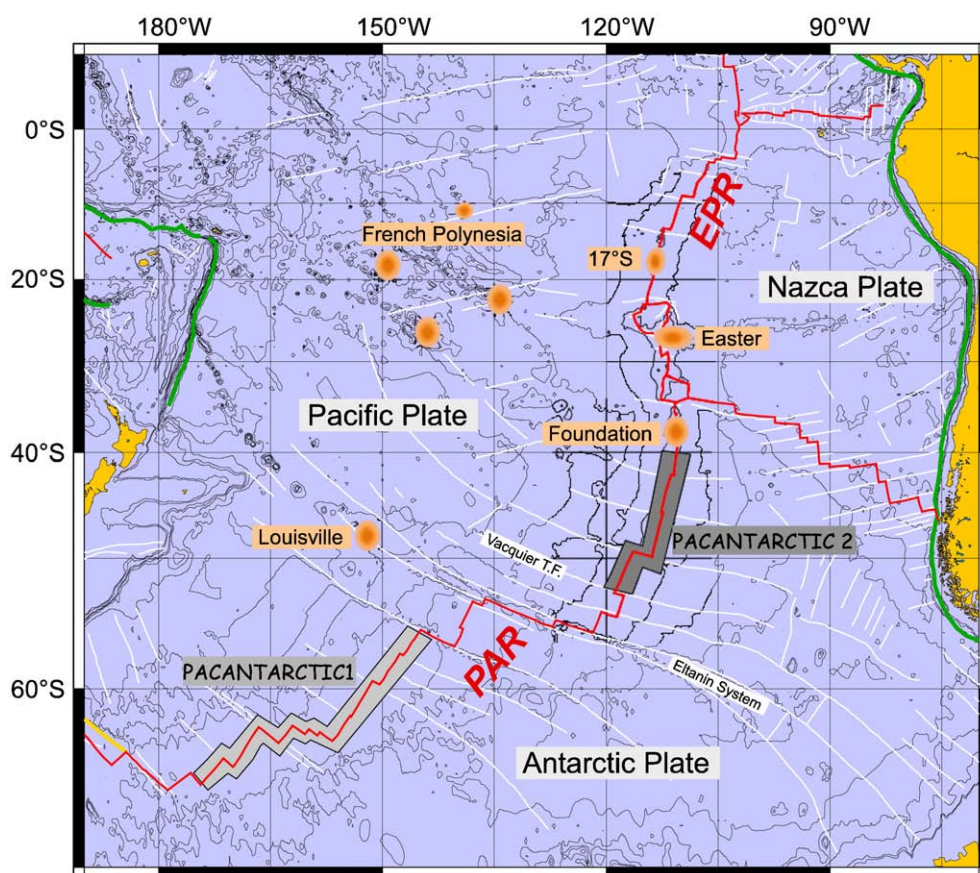
Fig. 1. Map of the south pacific basin showing the location of the PACANTARCTIC1 and PACANTARCTIC2 cruises with respect to the Pacific Antarctic Ridge (PAR) and the East Pacific Rise (EPR). Hotspot locations are shown in orange on the map.

22–35°N) could explain a decoupled behavior of $^{176}Hf/^{177}Hf$ with respect to other isotopic ratios. The linear correlations observed in our dataset show that the hypothesis of a specific behavior of Hf does not apply along the pacific ridges. Recently, good correlations between Hf and Nd isotopic ratios have been reported from other ridge segments such as Mohns Ridge (Blichert-Toft et al., 2005) and the entire mid-Atlantic Ridge (Agranier et al., 2005).

3.2. MORB variability along the south Pacific Ridge

Latitudinal isotopic variations of south Pacific Ridge basalts are shown in Fig. 3. An important geochemical feature from 66 to 10°S is a large-scale (spanning approximately 5000 km) and coherent variation of all isotopes shown by a bell shape grey line. The extremum of this variation defining the Pacific Isotopic Bump (PIB) is located at the latitude of Foundation (38°S). It reveals a less depleted component, characterized by more radiogenic values for Sr, Pb isotopic ratios, and correlatively less radiogenic values for Nd and Hf. Three shorter wavelength variations of the order of 200 to 700 km are seen as isotopic anomalies superimposed on the otherwise bell-shaped curve of the isotope signature along the ridge. In a way similar to the Pacific Isotopic Bump, these variations are towards more radiogenic Sr and Pb values and coherently less radiogenic Nd and Hf values. They indicate the influence of enriched materials due to plume–ridge interactions.

Helium isotopes do not fit this Sr–Pb/Hf–Nd coherent behavior. At the latitude of the Foundation–Ridge intersection (38°S), the bell-shaped He curve shows radiogenic $^{3}He/^{4}He$ ratios. But on the other hand, hot-spot influenced samples form negative "plume anomalies" with very unradiogenic signatures (high $^{3}He/^{4}He$ ratios, up to 12 R/Ra). The amplitudes of the PIB and the anomalies attributed to the plume effect are of the same order of magnitude for Nd, Hf, and Pb. For He and Sr, the PIB has much

smaller amplitude than the hotspot anomalies. Additionally, local MORB variability is expressed as spikes, which are likely related to transform faults (Eltanin System).

4. Discussion

4.1. Statistical definition of mantle reference lines

In most binary plots of radiogenic isotopic ratios, representative points of mantle derived material define linear trends. Historically, these trends have been used to define reference lines such as the Northern Hemisphere Reference Line (NHRL) in Pb–Pb plot (Hart, 1984) or the "Mantle Array" in Sr–Nd plot (DePaolo and Wasserburg, 1979) and the Nd–Hf plot (Vervoort and Blichert-Toft, 1999). These reference lines are arbitrary and depend on the abundance of data available at the time of their definition. However, the data colinearity in these plots justifies these convenient choices. The NHRL has been convenient to quantify the Dupal anomaly using the Δ7/4 and Δ8/4 (Hart, 1984). In 1999, new MORB data from the south Pacific lead to the definition of the Pacific Reference Line (PRL), which proved convenient to compare two sub-pacific mantle domains, using the δ(Nd–Sr) and δ(Sr–Pb) notations (Vlastélic et al., 1999). With the recent advance in analytical MC-ICPMS techniques, the number of isotopic data increases dramatically. It becomes possible to look at these reference lines in multidimensional space from a statistical point of view. Principal Component Analysis (PCA) is a powerful mathematical tool to study datasets such as a geochemical database including Sr–Nd–Pb–Hf analyses. The purpose of PCA analysis is to reduce the number of dimensions in a dataset by keeping those characteristics that contribute most to its variance. This technique has been used in previous mantle heterogeneity studies (e.g., Agranier et al., 2005, Debaille et al., 2006). The PCA method used with
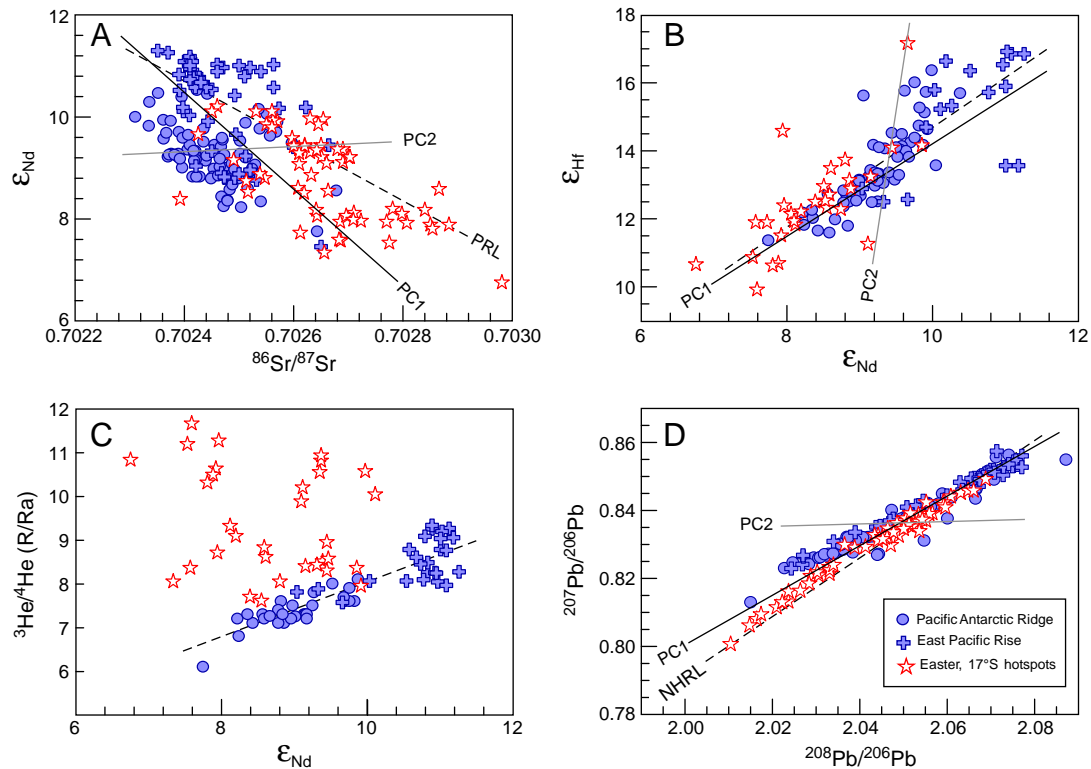
Fig. 2. Examples of binary plots showing correlations within the MORB field. Samples devoid of plume influence are shown in blue, whereas samples from plume–ridge interactions are in red. Blue circles represent samples collected along the PAR, and blue crosses, for EPR samples (all symbols are kept the same in all figures). Mantle reference lines defined in the literature are shown in dashed lines: in the Sr/Nd plot (A), the Pacific Reference Line (PRL) (Vlastélic et al., 1999), in the Nd/Hf plot (B), the mantle array (Vervoort and Blichert-Toft, 1999); in the Pb/Pb plot (D), the North Hemisphere Reference Line (NHRL) (Hart, 1984). Since no reference line had yet been recognized in plots involving He isotopes, we show here a regression line (^{3}He/^{4}He = 0.63 ε_{Nd} + 1.74, r = 0.89) (C). The projection of the two first principal components (PC1 and PC2) calculated in our study are shown (solid black and grey lines, see text for additional information). Data references can be found in supplementary materials.

our geochemical dataset has been initially developed for low-rank matrix approximations (Srebro and Jaakkola, 2003) and was recently adapted for tectonic problems using incomplete geodetic times series (Kositsky and Avouac, 2010). The main difference with traditional PCA methods is that the singular value decomposition is replaced by a more sophisticated decomposition, which appropriately takes into account samples with a missing isotope measurement. This technique is particularly suitable to geochemical data as it allows computing the principal components using the whole dataset, increasing therefore the accuracy of the calculation (see Supplementary material for a more detailed discussion about the concept and the limits of our calculation). Although more recently ICA (Independent Component Analysis) has been chosen by some authors (Iwamori and Albarède, 2008, Iwamori et al., 2010), the preferred PCA method used here has the advantage of dealing with missing isotopic data, assuming that decorrelation is still a good assumption of independence in our dataset.

Because the PCA method is an orthogonal linear transformation, it assumes the linearity of the data co-variations. In most binary isotopic diagrams, mixing processes are expressed by hyperboles whose curvatures depend on the elemental concentration ratios of the involved end-members. But in the case of MORB, pseudo-linear correlations are observed (Fig. 2) indicating that denominator elements are in approximately constant proportions in the mixing components. It is very difficult to evaluate the extent of non-linear relationships concealed within the analytical noise. However, it is worth noting that the geographical variations of the components calculated with our method are approximately the same as those computed in the 3-dimensional space of Pb isotopes, in which relationships are linear. In order to minimize the correlations induced by the ^{204}Pb analytical noise (it

represents only about 1.4% of the total Pb), the computation has been made in the ^{204}Pb/^{206}Pb, ^{207}Pb/^{206}Pb, and ^{208}Pb/^{206}Pb space. Considering the problematic of our study, this observation suggests that the curvature can be neglected. One drawback of PCA in general stems from the fact that PCA is a projection method, and sometimes low-dimensional visualization can lead to erroneous interpretations.

4.2. Distribution of the variance among the principal components

The most striking result of the PCA is that the first principal component accounts for more than 70% of the total variance. This result is remarkable considering the number of geochemical parameters involved in the very large number of samples used in this analysis. It indicates the strong coherence of all isotopic ratios within the depleted mantle domain. These correlations in binary plots of isotopic systems are the result of two antagonistic processes that took place over time: chemical fractionation events leading to the existence of enriched and depleted mantle reservoirs and mechanical mixing of theses reservoirs during mantle convection. The chemical fractionation between parent and daughter isotopes is controlled by distribution coefficients. Even if these coefficients can be modified by multiple parameters, they remain consistent from one element to another. Since these processes are approximately linear, the resulting dispersion is located along a line corresponding to PC1 (the first Principal Component).

While the importance of the first component is indisputable, one challenge with PCA is to establish the number of significant components needed to explain the observed data variance. A classical way to illustrate the number of relevant components is to study the residual variance (χ^2) obtained for each component (e.g., Kositsky and Avouac, 2010). This value
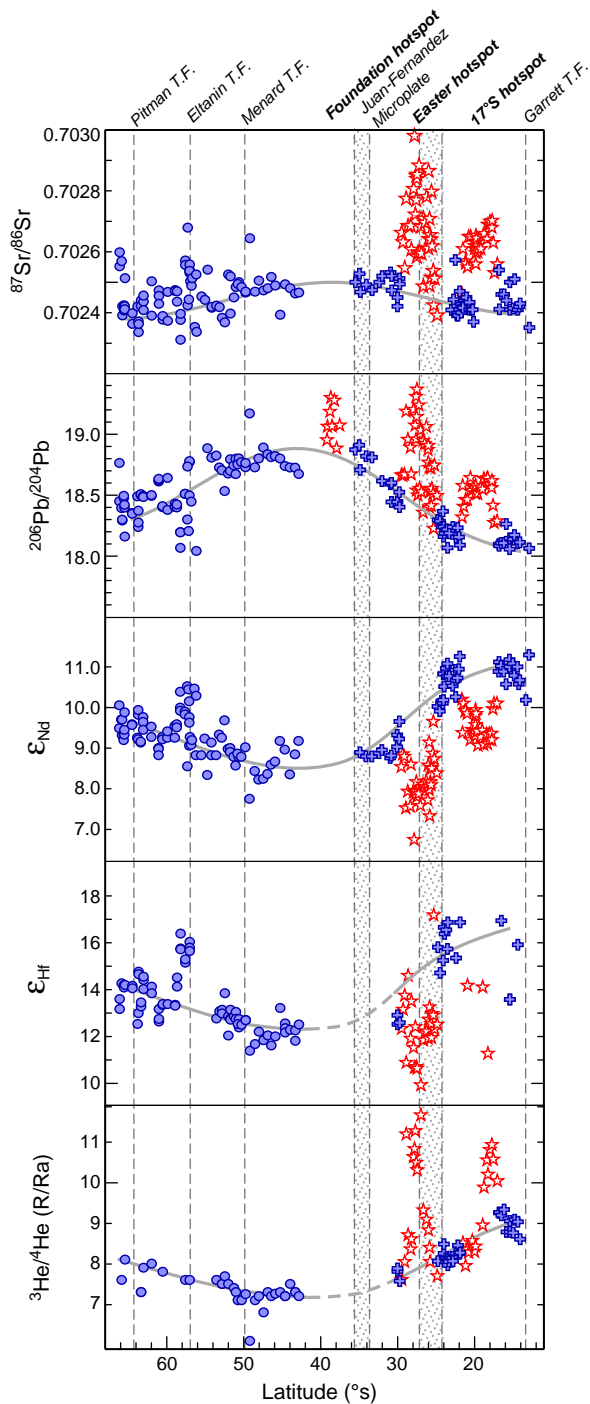
Fig. 3. Geochemical variations along the PAR and the EPR from 66°S to 10°S. Dashed lines represent the location of major transform faults in the area and a grey shade is used for the Juan Fernandez and Easter Island microplates. The grey curve underlines the large scale isotopic variation along the pacific ridges from 10 to 66°S and defines the Pacific Isotopic Bump (PIB).

drops abruptly after the third component (see Supplementary material). At first, we can infer that the information brought by the fourth to the sixth principal components is statistically insignificant and can safely be ignored. Using a PCA computed in the 3-dimensional space of Pb isotopes, the principal components account for 91.7%, 8.2%, and 0.1% of the variance for PC1, PC2, and PC3, respectively. This observation suggests that the variance expressed by principal components over the order of 2 is the result of a randomly distributed error. Also the absence of coherent geographical variation for the third component suggests that this variance

could either be a very local variation or an artifact of our data compilation (i.e., sampling bias, data and error normalization between different laboratories). This justifies to limit the discussion of the south pacific mantle heterogeneity to the PC1 and PC2 characteristics.

4.3. Mapping geochemical heterogeneities in the mantle using a PCA method

Using the dataset available at the time, Vlastélic et al. (1999) identified a large geochemical variation in the south Pacific depleted mantle. Based on an incomplete sampling of the ridge, they suggested the existence of a sharp boundary located at the latitude of the Easter Island Microplate (27°S). As an interpretation, they proposed that the Pacific Superswell divided the mantle into two domains each with their own convective histories, producing slight differences in their average isotopic signatures. More recently, the origin of these two domains has been challenged by a model based on plate kinetics (Small and Danyushevsky, 2003). Small and Danyushevsky proposed that geochemical discontinuities result from variations of the asthenosphere consumption, which corresponds to the ratio between the accretion rate and the spreading center migration relative to plumes. Their model predicted that the fast spreading, slowly migrating East Pacific Rise should have higher average melting degrees compared to the slower spreading, rapidly migrating Pacific–Antarctic Rise. In order to identify the two mantle domains along the Pacific Ridge, Vlastélic et al. (1999) used δ(Sr–Pb) and δ(Nd–Sr), which are defined as the vertical deviations from references lines in Pb vs. Sr and Sr vs. Nd isotopic ratio plots, respectively. These reference lines (see Section 4.1) were drawn intuitively in the greatest variance of their dataset. They can be directly compared to our first principal component. By construction, whatever the number of dimensions considered in the PCA, the projection of PC1 in a binary diagram resembles the relevant reference line (Fig. 2). Because PC2 is orthogonal to the greatest variance, sample values along this component are correlated to delta notations such as δ(Sr–Pb), δ(Nd–Sr), or Δ8/4Pb. But compared to delta notations, PC2 has the advantage of being rigorously and statistically determined in a multidimensional isotopic space. The application of the PCA method to our data compilation (excluding He isotopes) reveals a geochemical profile of the Pacific Ridge. The plot of PC1 versus latitude summarizes all the characteristics noted with the different isotopic systems (Fig. 4). The short-scale geochemical variations associated with hotspots as well as the large-scale variation are clearly visible. 17°S and 25°S (Easter Island) are well defined by sharp anomalies superimposed on the bell-shaped curve. A plot of PC2 versus latitude shows a very different picture (Fig. 4): only the large-scale variation is expressed by this component, the geochemical variations associated with hotspots are flattened and the corresponding samples are projected along the bell-shaped curve defining the Pacific Isotopic Bump. This PIB is also shown on plots of delta versus latitude, illustrating the equivalence of these parameters and PC2 (Fig. 4). At the Juan Fernandez/ Foundation latitude (36°S), the isotopic variation curve reaches an extreme which corresponds to a less "depleted" isotopic signature. In contrast with the conclusion of Vlastélic et al. (1999), we proposed that geochemical variations along the Pacific Ridge are not the result of two separated mantle domains but should rather be seen as a progressive variation of the isotopic composition of the sub-Pacific depleted mantle. Since the asthenosphere consumption varies abruptly at the Chile triple junction and is almost constant along the PAR, the plate kinematic model of Small and Danyushevsky (2003) is also inconsistent with the observed progressive variation of the MORB depleted matrix.

4.4. Mixing relationship within the depleted mantle compared to ridge-hotspot interactions

4.4.1. Asthenospheric versus hotspots signals as illustrated by Sr–Nd–Pb–Hf

Except in figures involving He isotopes, geochemical variations related to ridge/hotspot interactions are consistent with variations of samples devoid of plume influence. At first, it is difficult to distinguish the two types of variations in binary isotopic plots (Fig. 2). Nevertheless,
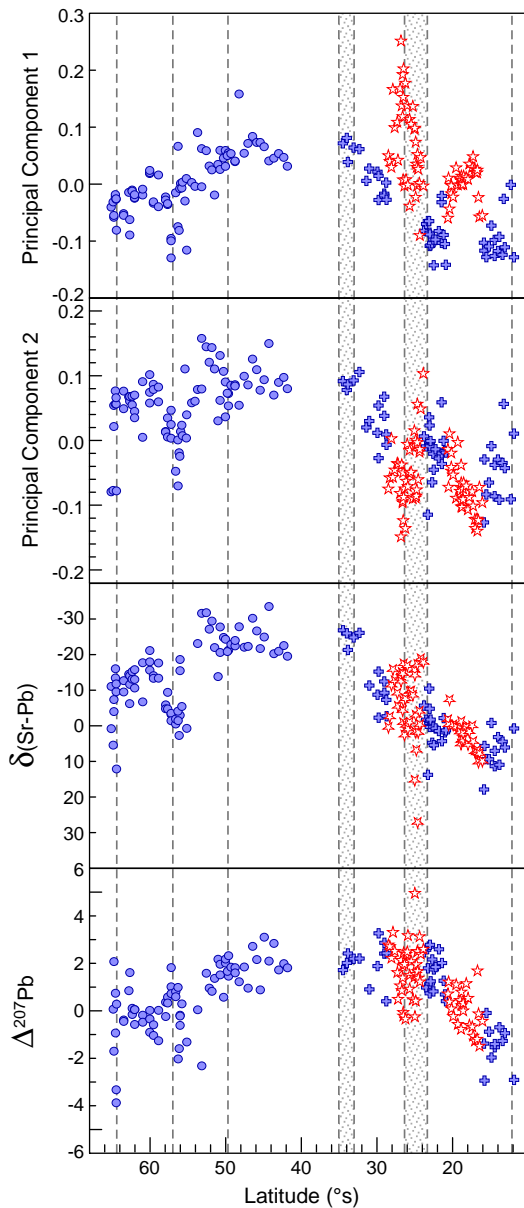
Fig. 4. Plot of the two first principal components along the Pacific Ridge. The similarity between PC2 and δ notation is illustrated by plotting δ(Sr–Pb) as defined by Vlastélic et al. (1999) and $\Delta^{207}Pb$ as defined by Hart (1984) versus latitude.

trends. Nevertheless, the PCA calculations establish that the progressive geochemical change of the depleted matrix of the Pacific mantle is not the result of hotspot material being diluted into the depleted mantle. Using a different approach, Meyzen et al. (2007) successfully unscrambled the hotspot and asthenospheric signals. These authors have proposed that the geochemical variations unrelated to ridge/ hotspot interactions along the South West Indian ridge and the South Atlantic ridge are related to a broad lower mantle upwelling in this area. Similarly, a broad lower mantle input could be a plausible cause of the Pacific Isotopic Bump associated with the high spreading rates in the vicinity of the Chile Ridge Triple junction.

It is interesting to compare the results of our PCA calculation along the Pacific ridge with the spectral analysis performed along the Atlantic ridge by Agranier et al. (2005). These authors found two contrasting types of spectra along their study area. The first type is associated with ridge–hotspot interactions and is seen in the first principal component. The second type is illustrated by the continuous power decrease with the decreasing wavelength of the second principal component. Agranier et al. (2005) have interpreted this second type of spectra, unrelated to hotspots, as being the result of the continuous size reduction of mantle heterogeneities upon stretching and refolding of the convecting mantle. Despite the differences in geological settings between the Pacific ridge and the Atlantic ridge, our observations are in good agreement with the statistical analysis of Agranier et al. (2005). We view the PIB as the consequence of a progressive change in the relative proportions of the marble-cake components present in the Pacific upper mantle. In this model, hotspot anomalies are superimposed on the intrinsic mantle heterogeneity expressed in MORB.

4.4.2. He isotopes in the depleted mantle compared to hotspot signals

Unlike other isotopic systems, helium shows a first order discrepancy between the hotspot and the depleted mantle signals in our studied area (Figs. 3 and 6): the large-scale variation associated to the depleted mantle is characterized by an increase towards more radiogenic (low $^3He/^4He$) compositions, whereas the short-scale variation associated to the mantle plumes points towards high $^3He/^4He$ values as previously noted in Hanan and Graham (1996). The origin of the large range of elevated $^3He/^4He$ values in OIB lavas is a long-lived controversial question (Allègre et al., 1983; Kurz et al., 1982; Meibom et al., 2003; Allègre and Moreira, 2004). Historically, the requirement of a high $^3He/^4He$ reservoir for the OIB leads to the idea that plumes are tapping a deep, undegassed lower mantle, isolated from the upper mantle convection (Allègre, 1997; O'Nions et al., 1996). Numerous alternative models have tried to solve the apparent inconsistency between the high $^3He/^4He$ ratio in plumes and the requirement of a source previously processed through partial melting

a PCA computed with all heavy radiogenic isotopes clearly illustrates a difference: hotspot signatures are exclusively visible with PC1, while the variance related to the large-scale variation (PIB) is illustrated by both PC1 and PC2 versus latitude (Fig. 4). In PC1 versus PC2 space, the MORB field extends from the depleted end member of the mantle (DMM) toward a recycled oceanic crust end member with a HIMU affinity (Fig. 5). The samples identified as resulting from a plume–ridge interaction are not part of this "depleted trend". Rather their data field extends from the depleted trend towards more enriched-type end members such as C and/or EM. This observation supports the idea that the large-scale variation in the depleted Pacific mantle is unrelated to ridge/hotspot interactions. This variation is therefore equivalent to the intrinsic variability of MORB recognized in other areas (e.g., Dosso et al., 1999; Donnelly et al., 2004; Debaille et al., 2006; Hémond et al., 2006). It has to be noted that PCA calculations assume linearity criteria, which are not satisfied when dealing with isotopic compositions of the mantle end-members. It is thus not possible to determine more precisely the nature of the different mantle components responsible for the observed
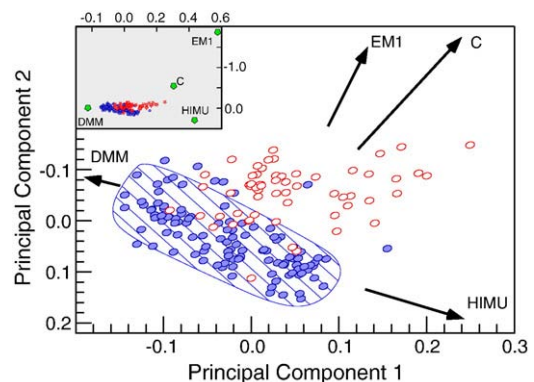

Fig. 5. Plot of PC2 versus PC1 for a principal component analysis computed using Sr, Nd, Hf, and Pb isotopes. The hashed blue field defines the depleted trend and includes EPR and PAR samples. Data points are drawn as ellipses representing the 95% confidence domain of the components as calculated in Debaille et al. (2006). The insert shows the location of the classical mantle end-members in the PC2 vs PC1 space.

(e.g., Albarède, 2008; Class and Goldstein, 2005; Davies, 2010; Parman et al., 2005; Putirka, 2008).

Compared to plume-influenced samples, systematics of He isotopes in depleted MORB samples have shown a very restricted range of $^3He/^4He$ with a peak of distribution around 8 ± 1 (R/Ra) (Graham, 2002). Within the uncontaminated depleted mantle sampled along our studied area, $^3He/^4He$ varies from 6 to 9.5 (R/Ra). Samples devoid of plume influence fall along a negative trend toward low $^3He/^4He$ values and high $^{206}Pb/^{204}Pb$. This variation of He isotopes in our samples devoid of plume influence is clearly related to the PIB identified along the pacific ridge using PCA with Sr, Nd, Pb, and Hf isotopes. It is interesting to note that the most enriched samples from this correlation show the lowest $^3He/^4He$ values (more radiogenic). In order to reconcile the $^3He/^4He$ variations with variations of Sr, Pb, Nd, and Hf isotopes, new models take into account the physical specificities of He compared to heavy radiogenic isotopes: its diffusivity in mantle conditions and its capacity to be outgassed from melts at sub-surface pressure (e.g., Albarède, 2008; Gonnermann and Mukhopadhyay, 2009; Hart et al., 2008). We propose that the melting of a marble-cake upper mantle, unpolluted by plumes, produces the good correlation observed between He and Pb isotopes in our depleted samples. The less depleted component of the mantle assemblage is characterized by a high Pb isotopic ratio and a low $^3He/^4He$ ratio. We suggest that this component was derived from the recycling of an extensively outgassed oceanic crust. When the oceanic crust is subducted back into the mantle, it contains negligible concentration of mantle-derived He (Staudacher and Allègre, 1988). With time, this very low $^3He/(U+Th)$ in subducted slabs is expected to produce the end-member with high Pb isotopes value and low $^3He/^4He$ ratio (Fig. 6).

In our model, the variation of He isotopes along the pacific ridge could be interpreted as (1) a smaller contribution of the refractory layers (less radiogenic), corresponding to a lower $^3He/^4He$ ratio at the PIB but because the melting rate is expected to be higher near the Chile Ridge Triple Junction, this hypothesis seems very unlikely, or (2) a higher volume of the recycled end-member in this area. This hypothesis is in agreement with the conclusions derived from the PCA based on heavy radiogenic isotopes (Section 4.4.1). The intrinsic geochemical variation of the depleted upper mantle comforts the image of a marble cake mantle composed of a refractory component and a recycled oceanic crust component. A broad volume of recycled component associated with the high spreading rates in the vicinity of the Chile Ridge Triple junction is therefore a plausible cause of the Pacific Isotopic Bump. The correlation between He and Pb isotopes revealed by our new data (Fig. 6) suggests that the depleted mantle is the outcome of a mixing of a different nature that the one involved in the plume–ridge interaction.
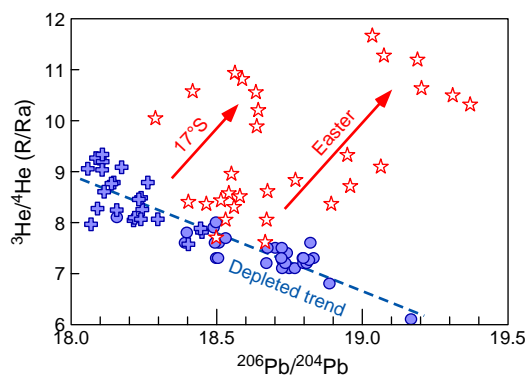

Fig. 6. Binary plot of $^3He/^4He$ vs $^{206}Pb/^{204}Pb$. The dashed regression line ($^3He/^4He = -2.33$ $^{206}Pb/^{204}Pb + 51.0$) is defined by samples devoid of plume influence. Plume–ridge interactions (17°S and Easter hotspots) are characterized by positive trends emerging from the PAR-EPR array and pointing towards higher $^3He/^4He$ (R/Ra) ratios and higher $^{206}Pb/^{204}Pb$.

5. Conclusion

Analyses of this new sampling of the PAR complete the dataset of the Pacific Ridge. Therefore, it becomes possible to have a picture of the geochemical variations from 10 to 70°S. Our data show a clear geographical evolution of isotopic characteristics along the Pacific Ridge. In binary isotopic plots, this large-scale variation is expressed by correlations between each isotopic dimension. This observation holds true even for the Nd–Hf system previously reported as decoupled for MORB samples (Debaille et al., 2006). Even more significant in this study is the linear correlation shown in the isotopic He–Nd and $^3He/^4He$–$^{206}Pb/^{204}Pb$ plots. In these isotopic spaces, the samples affected by plume–ridge interactions depart clearly from the linear correlations displayed by the ridge samples coming from the depleted mantle.

Despite the paucity of combined Sr–Nd–Pb–Hf isotope data on individual samples, the PCA algorithms used here allow us to portray the variation along a huge section of the Pacific Ridge from a statistical point of view. Compared to previous studies of the sub-Pacific mantle, the application of PCA reveals a Pacific Isotopic Bump, which can be seen as a progressive geochemical variation of the depleted upper mantle matrix rather than a sharp frontier between two mantle domains. Combining PCA results with the information given by He isotopes, we suggest that the Pacific Isotopic Bump is unrelated to plume–ridge interactions. This geochemical variation in the upper mantle reservoir is the result of a marble-cake mantle assemblage composed of a residual mantle component and a recycled oceanic crust component.

References

Agranier, A., Blichert-Toft, J., Graham, D., Debaille, V., Schiano, P., Albarede, F., 2005. The spectra of isotopic heterogeneities along the mid-Atlantic Ridge. Earth Planet. Sci. Lett. 238 (1–2), 96–109.
Albarède, F., 2001. Radiogenic ingrowth in systems with multiple reservoirs: applications to the differentiation of the mantle-crust system. Earth Planet. Sci. Lett. 189 (1–2), 59–73.
Albarède, F., 2008. Rogue mantle Helium and Neon. Science 319, 943–945.
Allègre, C.J., Staudacher, T., Sarda, P., Kurz, M., 1983. Constraints on evolution of the earth's mantle from rare gas systematic. Nature 303, 762–766.
Allègre, C.J., 1997. Limitation on the mass exchange between the upper and lower mantle: the evolving convection regime of the Earth. Earth Planet. Sci. Lett. 150 (1–2), 1–6.
Allègre, C.J., Moreira, M., 2004. Rare gas systematics and the origin of oceanic islands: the key role of entrainment at the 670 km boundary layer. Earth Planet. Sci. Lett. 228, 85–92.
Blichert-Toft, J., Albarède, F., 1999. Hf isotopic compositions of the Hawaii Scientific Drilling Project core and the source mineralogy of Hawaiian basalts. Geophys. Res. Lett. 26 (7), 935–938.
Blichert-Toft, J., Agranier, A., Andres, M., Kingsley, R., Schilling, J.-G., Albarède, F., 2005. Geochemical segmentation of the Mid-Atlantic Ridge north of Iceland and ridge-hot spot interaction in the North Atlantic. Geochem. Geophys. Geosyst. 6 (1), Q01E19.
Cande, S.C., Raymond, C.A., Stock, J., Haxby, W.F., 1995. Geophysics of the Pitman fracture zone and Pacific–Antarctic plate motions during the Cenozoic. Science 270, 947–953.
Castillo, P., 1998. The Dupal anomaly as a trace of the upwelling lower mantle. Nature 336, 667–670.
Chauvel, C., Blichert-Toft, J., 2001. A hafnium isotope and trace element perspective on melting of the depleted mantle. Earth Planet. Sci. Lett. 190 (3–4), 137–151.

Class, C., Goldstein, S., 2005. Evolution of helium isotopes in the Earth's mantle. Nature 436 (25), 1107–1112.

Cooper, K.M., Eiler, J.M., Sims, K.W.W., Langmuir, C.H., 2009. Distribution of recycled crust within the upper mantle: insights from the oxygen isotope composition of MORB from the Australian–Antarctic Discordance. Geochem. Geophys. Geosyst. 10.

Davies, 2010. Noble gases in the dynamic mantle. Geochem. Geophys. Geosyst. 11 (3), Q03005.

Debaille, V., Blichert-Toft, J., Agranier, A., Doucelance, R., Schiano, P., Albarède, F., 2006. Geochemical component relationships in MORB from the Mid-Atlantic Ridge, 22–35°N. Earth Planet. Sci. Lett. 241 (3–4), 844–862.

DePaolo, D.J., Wasserburg, G.J., 1979. Sm–Nd age of the Stillwater complex and the mantle evolution curve for neodymium. Geochim. Cosmochim. Acta 43, 999–1008.

Donnelly, K.E., Goldstein, S.L., Langmuir, C.H., Spiegelman, M., 2004. Origin of enriched ocean ridge basalts and implications for mantle dynamics. Earth Planet. Sci. Lett. 226, 347–366.

Dosso, L., Bougault, H., Langmuir, C., Bollinger, C., Bonnier, O., Etoubleau, J., 1999. The age and distribution of mantle heterogeneity along the Mid-Atlantic Ridge (31–41°N). Earth Planet. Sci. Lett. 170, 269–286.

Dosso, L., Ondréas, H., Briais, A., Fernagu, P., Floch, G., Hamelin, C., Hanan, B.B., Klingelhoefer, F., Moreira, M., Normand, A., 2005. The Pacific–Antarctic Ridge between 41°15′S and 52°45′S: survey and sampling during the PACANTARCTIC 2 cruise. Inter Ridge News 14, 1–5.

Dupré, B., Allègre, C.J., 1983. Pb–Sr isotope variation in Indian Ocean basalts and mixing phenomena. Nature 303, 142–146.

Gonnermann, H.M., Mukhopadhyay, S., 2009. Preserving noble gases in a convecting mantle. Nature 459, 560–563.

Graham, D.W., 2002. Noble gas isotope geochemistry of mid-ocean ridge and ocean island basalts: characterization of mantle source reservoirs. In: Noble Gases in Geochemistry and Cosmochemistry, Reviews in Mineralogy and Geochemistry, Mineral. Soc. Amer., Washington, D.C. 47, 247–319.

Hamelin, C., Dosso, L., Hanan, B., Barrat, J.-A., Ondréas, H., 2010. Sr–Nd–Hf isotopes along the Pacific Antarctic Ridge from 41 to 53°S. Geophys. Res. Lett. 37 (10), L10303.

Hanan, B.B., Graham, D.W., 1996. Lead and helium isotope evidence from oceanic basalts for a common deep source of mantle plumes. Science 272, 991–995.

Hanan, B.B., Blichert Toft, J., Pyle, D.G., Christie, D.M., 2004. Contrasting origins of the upper mantle revealed by hafnium and lead isotopes from the Southeast Indian Ridge. Nature 432, 91–94.

Hart, S.R., 1984. A large scale isotope anomaly in the Southern Hemisphere mantle. Nature 309, 753–757.

Hart, S.R., Kurz, M.D., Wang, Z., 2008. Scale length of mantle heterogeneities: constraints from helium diffusion. Earth Planet. Sci. Lett. 269 (3–4), 508–517.

Hémond, C., Hofmann, A.W., Vlastélic, I., Nauret, F., 2006. Origin of MORB enrichment and relative trace element compatibilities along the Mid-Atlantic Ridge between 10° and 24°N. Geochem. Geophys. Geosyst. 7, Q12010.

Hofmann, A.W., 2003. Sampling mantle heterogeneity through oceanic basalts: isotopes and trace elements. In: Holland, H., Turekian, K.K. (Eds.), Treatise on Geochemistry. Elsevier-Pergamon, Oxford, pp. 61–101.

Iwamori, H., Albarède, F., 2008. Decoupled isotopic record of ridge and subduction zone processes in oceanic basalts by independent component analysis. Geochem. Geophys. Geosyst. 9.

Iwamori, H., Albarède, F., Nakamura, H., 2010. Global structure of mantle isotopic heterogeneity and its implications for mantle differentiation and convection. Earth Planet. Sci. Lett. 299 (3–4), 339–351.

Ishizuka, O., Taylor, R.N., Milton, J.A., Nesbitt, R.W., 2003. Fluid-mantle interaction in an intra-oceanic arc: constraints from high-precision Pb isotopes. Earth Planet. Sci. Lett. 211, 221–236.

Kellogg, J.B., Jacobsen, S.B., O'Connell, R.J., 2007. Modeling lead isotopic heterogeneity in mid-ocean ridge basalts. Earth Planet. Sci. Lett. 262 (3–4), 328–342.

Klingelhoefer, F., Ondréas, H., Briais, A., Hamelin, C., Dosso, L., 2006. New structural and geochemical observations from the Pacific–Antarctic Ridge 52°45'S and 41°15'S. Geophys. Res. Lett. 33.

Kositsky, A.P., Avouac, J.P., 2010. Inverting geodetic time series with a principal component analysis-based inversion method. J. Geophys. Res. 115 (B3), B03401.

Kurz, M.D., Jenkins, W.J., Hart, S.R., 1982. Helium isotopic systematics of oceanic islands and mantle heterogeneity. Nature 297, 43–47.

Lonsdale, P., 1994. Geomorphology and structural segmentation of the crest of the southern (Pacific–Antarctic) East Pacific Rise. J. Geophys. Res. 99 (B3), 4683–4702.

Meibom, A., Anderson, D.L., Sleep, N.H., Frei, R., Chamberlain, C.P., Hren, M.T., Wooden, J.L., 2003. Are high 3He/4He ratios in oceanic basalts an indicator of deep-mantle plume components? Earth Planet. Sci. Lett. 208 (3–4), 197–204.

Meibom, A., Anderson, D.L., 2004. The statistical upper mantle assemblage. Earth Planet. Sci. Lett. 217 (1–2), 123–139.

Meyzen, C.M., Ludden, J.N., Humler, E., Luais, B., Toplis, M.J., Mével, C., Storey, M., 2005. New insights into the origin and distribution of the DUPAL isotope anomaly in the Indian Ocean mantle from MORB of the Southwest Indian Ridge. Geochem. Geophys. Geosyst. 6 (11), 1–34.

Meyzen, C.M., Blichert-Toft, J., Ludden, J.N., Humler, E., Mevel, C., Albarede, F., 2007. Isotopic portrayal of the Earth/'s upper mantle flow field. Nature 447 (7148), 1069–1074.

Moreira, M., Staudacher, T., Sarda, P., Schilling, J.-G., Allègre, C.J., 1995. A primitive plume neon component in MORB: the Shona ridge-anomaly, South Atlantic (51–52°S). Earth Planet. Sci. Lett. 133, 367–377.

Moreira, M., Dosso, L., Ondréas, H., 2008. Helium isotopes on the Pacific–Antarctic ridge (52.5–41.5°S). Geophys. Res. Lett. 35 (L10306), 1–6.

Ondréas, H., Aslanian, D., Géli, L., Olivet, J.-L., Briais, A., 2001. Variations in axial morphology, segmentation, and seafloor roughness along the Pacific–Antarctic Ridge between 56°S and 66°S. J. Geophys. Res. 106 (B5), 8521–8546.

O'Nions, R.K., Peltier, W.R., Davies, J.H., Runcorn, S.K., 1996. Phase-transition modulated mixing in the mantle of the Earth—discussion. Philos. Trans. R. Soc. London, Ser. A - Math. Phys. Eng. Sci. 354 (1711), 1443–1447.

Parman, S.W., Kurz, M.D., Hart, S.R., Grove, T.L., 2005. Helium solubility in olivine and implications for high 3He/4He in ocean island basalts. Nature 437 (7062), 1140–1143.

Patchett, P.J., Tatsumoto, M., 1980. Hafnium isotope variations in oceanic basalts. Geophys. Res. Lett. 7, 1077–1080.

Putirka, K., 2008. Excess temperatures at ocean islands: implications for mantle layering and convection. Geology 36 (4), 283–286.

Pyle, D.G., Christie, D.M., Mahoney, J.J., 1992. Resolving an isotopic boundary within the Australian–Antarctic Discordance. Earth Planet. Sci. Lett. 112, 161–178.

Rudge, J.F., McKenzie, D., Haynes, P.H., 2005. A theoretical approach to understanding the isotopic heterogeneity of mid-ocean ridge basalt. Geochim. Cosmochim. Acta 69 (15), 3873–3887.

Salters, V.J.M., White, W.M., 1998. Hf isotope constraints on mantle evolution. Chem. Geol. 145, 447–460.

Small, C., Danyushevsky, L.V., 2003. Plate-kinematic explanation for mid-oceanic-ridge depth discontinuities. Geology 31 (5), 399–402.

Srebro, N.N., Jaakkola, T., 2003. Weighted low-rank approximations, paper presented at 20th International Conference on Machine Learning. Assoc. for the Adv. of Art. Intell, Washington, D. C.

Staudacher, T., Allègre, C.J., 1988. Recycling of oceanic crust and sediments: the noble gas subduction barrier. Earth Planet. Sci. Lett. 89 (2), 173–183.

Vlastélic, I., Aslanian, D., Dosso, L., Bougault, H., Olivet, J.L., Géli, L., 1999. Large-scale chemical and thermal division of the Pacific mantle. Nature 399 (6734), 345–350.

Vlastélic, I., Dosso, L., Bougault, H., Aslanian, D., Géli, L., Etoubleau, J., Bohn, M., Joron, J.L., Bollinger, C., 2000. Chemical systematics of an intermediate spreading ridge: the Pacific–Antarctic Ridge between 56°S and 66°S. J. Geophys. Res. 105 (B2), 2915–2936.

Vervoort, J.D., Blichert-Toft, J., 1999. Evolution of the depleted mantle: Hf isotope evidence from juvenile rocks through time. Geochim. Cosmochim. Acta 63, 553–556.